

Zero-shot sketch-based remote sensing image retrieval based on multi-level and attention-guided tokenization

Bo Yang, Chen Wang, *Member, IEEE*, Xiaoshuang Ma, *Member, IEEE*, Beiping Song and Zhuang Liu

Abstract— Effectively and efficiently retrieving images from remote sensing databases is a critical challenge in the realm of remote sensing big data. Utilizing hand-drawn sketches as retrieval inputs offers intuitive and user-friendly advantages, yet the potential of multi-level feature integration from sketches remains underexplored, leading to suboptimal retrieval performance. To address this gap, our study introduces a novel zero-shot, sketch-based retrieval method for remote sensing images, leveraging multi-level, attention-guided tokenization. This approach starts by employing multi-level self-attention feature extraction to tokenize the query sketches, as well as self-attention feature extraction to tokenize the candidate images. It then employs cross-attention mechanisms to establish token correspondence between these two modalities, facilitating the computation of sketch-to-image similarity. Our method demonstrates superior retrieval accuracy over existing sketch-based remote sensing image retrieval techniques, as evidenced by tests on four datasets. Notably, it also exhibits robust zero-shot learning capabilities and strong generalizability in handling unseen categories and novel remote sensing data. The method's scalability can be further enhanced by the pre-calculation of retrieval tokens for all candidate images in a database. This research underscores the significant potential of multi-level, attention-guided tokenization in cross-modal remote sensing image retrieval. For broader accessibility and research facilitation, we have made the code and dataset used in this study publicly available online. Code and dataset are available at <https://github.com/Snowstormfly/Cross-modal-retrieval-MLAGT>.

Index Terms—Remote sensing image retrieval, zero-shot learning, attention mechanism, deep learning, transformers.

I. INTRODUCTION

THE proliferation of remote sensing sensors deployed on various carrier platforms has led to a continuous and rapid increase in the volume of observation data pertaining to the Earth's surface. The data generated by these

sensors possesses the characteristics commonly associated with big data: it is voluminous, exhibits a wide variety, is generated at high velocity, and requires rigorous verification. While this abundance of data offers users unprecedented opportunities to discover and quantify underlying phenomena, it also presents many challenges [1]-[3]. One of the most prominent challenges pertains to the effective and efficient extraction of images of interest from within remote sensing data warehouses, which is essential for subsequent data mining processes [4]. Traditional query inputs typically involve image metadata values, such as bounding box coordinates, sensor names, and timestamps. Another commonly employed approach, which is content-based remote sensing image retrieval (CBRSIR) involves querying remote sensing warehouses using example images, often yielding promising results when coupled with state-of-the-art deep learning algorithms [5], [6]. However, in numerous application scenarios, users encounter difficulty in providing desirable remote sensing examples. Consequently, some cross-model retrieval method, such as text-image retrieval [7] and sketch-based remote sensing image retrieval (SBRISIR) [8] has captured the attention of some researchers. As demonstrated in Figure 1. SBRISIR offers users the ability to express the structure of a desired remote sensing image from their mind through freehand sketches, which can then be employed as queries for retrieving images. This method is believed to be intuitive for users, easy to execute on touch-enabled devices, and capable of achieving a high level of expressiveness and flexibility [9]-[12].

While Sketch-based image retrieval (SBIR) and Zero Shot SBIR (ZS-SBIR) for common images have undergone extensive investigation in recent years and yielded promising results [13]-[17], their application to remote sensing images remains relatively limited, with only a small number of recent research publications addressing the topic [8], [18]-[22]. The substantial differences in patterns and structures between remote sensing images and typical photos or pictures often pose challenges when directly applying SBIR algorithms and models. Consequently, researchers in the field of remote sensing applications often find themselves compelled to design and train ad-hoc models. There are two primary challenges in the domain of SBRISIR. First, there is an extensive array of categories concerning objects and scenes within remote sensing images. Also, the sketch samples are largely scarce, compared with the ordinary photo-related sketches [8]. As a result, constructing a comprehensive

This work was supported in part by the National Natural Science Foundation of China under Grants 41901410. Natural Science Research Project of Anhui Educational Committee under Grants 2023AH050103. (Corresponding author: Chen Wang and Xiaoshuang Ma, email: chen.wang@ahu.edu.cn; mxs.88@whu.edu.cn).

B. Yang, C. Wang, X. Ma, and B. Song are with Anhui Province Key Laboratory of Wetland Ecosystem Protection and Restoration, Anhui University, Hefei 230601, China, and also with the Department of Resources and Environmental Engineering, Anhui University, Hefei, China.

L. Zhuang is with Shanghai Ubiquitous Navigation Technology Co. Ltd. (email: liuz@ubinavi.com.cn).

training dataset for remote sensing SBIR proves to be a formidable task. In contrast to the general image processing domain, well-annotated datasets for remote sensing images and sketches remain insufficient for supervised learning [18], thus, potentially affecting the performance of trained networks, particularly when confronted with unseen categories and images. Given the challenges associated with significantly expanding training datasets to encompass all potential categories and data sources in remote sensing, existing SBRSIR research underscores the importance of zero-shot

learning performance [18], [19]. Nevertheless, the existing models in this domain still exhibit very limited zero-shot capabilities. The second challenge is that remote sensing images exhibit distinct characteristics depending on the sensor and their carrier platform. The SBRSIR model should have a good generalization capability to support different sources of remote sensing images. However, current work investigated very little in the generalization capability of the SBRSIR model.

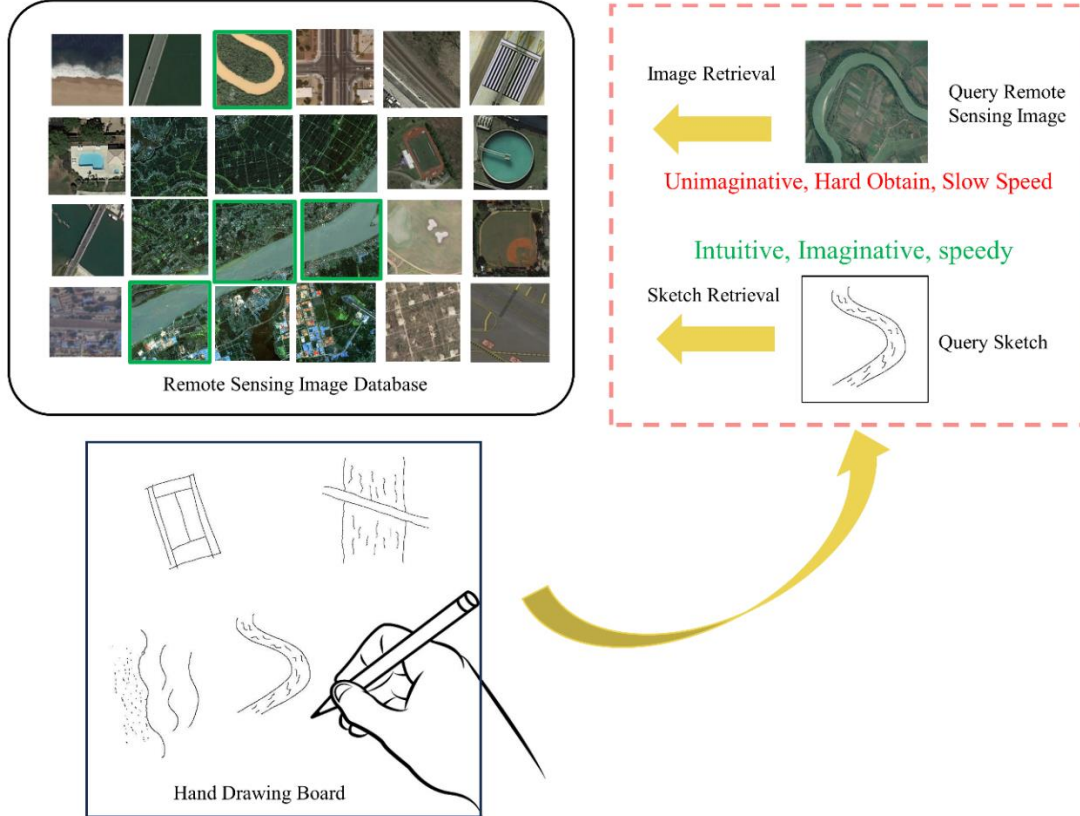


Fig. 1. Demo of sketch-based remote sensing image retrieval process and its advantages compared to content-based retrieval.

In response to the growing demand and challenges of SBRSIR, we propose a novel zero-shot cross-model deep learning network that leverages a new multi-level feature acquisition and attention-guided tokenization mechanism. Additionally, we have substantially expanded the RSketch SBRSIR benchmark dataset to serve as a comprehensive testbed, allowing for a comprehensive evaluation of the performance of our new method in various settings, including images from both seen and unseen categories and data sources. Our test results reveal that our new method significantly outperforms existing SBRSIR algorithms. Our proposed algorithm exhibits excellent zero-shot capabilities, enabling precise retrieval of images from unseen categories, and demonstrates strong generalization capabilities, as it can be trained on mixed-source remote sensing image samples and retrieve images from previously unseen data sources, thereby offering extensive application flexibility.

The main contributions and innovations of our proposed method can be summarized in two key aspects:

1) We introduce a novel deep learning SBRSIR network equipped with a multi-level feature acquisition and attention-guided tokenization mechanism. This new approach has demonstrated substantial performance improvements compared to existing methods, particularly in terms of its good zero-shot capability. Furthermore, our proposed model showcases impressive generalization capabilities as it can be trained using mixed-source remote sensing datasets and can retrieve remote sensing image from unseen sources.

2) We have substantially expanded SBRSIR benchmark RSketch dataset to RSketch_ext dataset as testbed. This new testbed encompasses 20 categories, each containing 90 sketches and over 400 remote sensing images from various datasets. We have made this comprehensive dataset as well as the code of our method available online to facilitate the work of researchers in this field.

The rest of this article is organized as follows. Section II describes the related work of SBRSIR. Section III gives the details of our proposed method. Some experimental results are

reported in Section IV. The discussion is given in Section V and conclusion is drawn in Section VI.

II. RELATED WORKS

This section explores prior research in the field of SBIR, SBRSIR, and other application domains within image retrieval. The utilization of freehand-drawn sketches as input queries has attracted researchers in computer vision [23], [24], human-computer interaction [25], and geographical information science [26] since its early stages. The inherent challenge in sketch-based retrieval lies in the multi-modality nature of such a task. Sketches significantly differ from photographic or remote sensing images due to their abstract, symbolic, sparse, and stylistic nature, often containing rich topological and semantic information.

SBIR can be categorized into two levels in terms of granularity: categorical [27] and fine-grained [28]. Categorical SBIR focuses on recognizing the categorical information in sketches, retrieving images from the same category, often described by semantic notions like "plane". In remote sensing domain, the development is currently at a categorical level [8], [18]. On the other hand, fine-grained or instance-level SBIR delves into scene and stroke details, such as relative location and topology, for more precise image retrieval. Both categorical and fine-grained SBIR may frequently encounter images from unseen categories during testing. To address this, Zero-Shot Learning (ZSL) algorithms are introduced, often employing assisting information such as word embeddings [18], [29], [30] for semantic similarity measurement. Recent works aim to enhance algorithm's generalizability, adopting features and local correspondence information for fine-grained yet generalizable algorithms [13], [31]. The improvement of algorithms' generalizability may also be helpful in cross-dataset retrieval [13]. Despite advancements in computer vision domain, such algorithms have not been explored in the context of sketch-based retrieval in the remote sensing domain.

A. Cross-Model Feature Extraction

Most contemporary SBIR and SBRSIR algorithms generally follow a three-part pipeline: cross-model feature extraction, feature enhancement, and image retrieval. The feature extraction part extract informative and representative features from both sketches and images of other modalities. Initially, hand-crafted features like gradient field HOG [23], edge maps [32], and histogram of edge local orientations [33] were applied. However, recent years have seen the widespread adoption of deep learning [9], [34] in SBIR and SBRSIR [21], [22], outperforming handcrafted methods [35]. Various deep network structures, including FCN [36], CNN [37], RNN [24], VAE [38], GNN [39], transformers [40], and ViT [13], have been explored. The latest solutions often combine multiple deep structures [13], [37] and employ homogeneous [41], Siamese branch [9], or heterogeneous structures [42] for different modalities.

B. Feature Enhancement

Feature enhancement part involves feature selection, aggregation, and embedding [16]. It prepares the extracted

feature for comparison and retrieval. Recent content-based image retrieval research [43], [44] utilizes attention maps to weigh feature importance, with [45] proposing feature elimination or merging for efficiency without significant accuracy loss—a novel approach in SBIR. For feature embedding, common methods include Bag of features [46], Bag of visual words [23], VLAD [47], and FV [48]. To enhance scalability, deep features could be pre-calculated and embedded in binary hash codes [49], [50].

C. Image Retrieval

After encoding features in the embedding space, image retrieval typically involves a Nearest Neighbor search based on global similarity calculated through Euclidean distance [51] or Hamming distance for binary hash codes [52]. Deep metric learning is also prevalent in similarity calculation in SBIR [53], [54]. Instead of global similarity calculation, some works focus on local matching pairs between sketches and images for similarity scoring, such as [55] using the quantity of matching pairs and [13] employing a cosine similarity matrix. Approaches like Deep Hashing [49], Approximate Nearest Neighbor (ANN) using k-means tree [56], and ANN using product-quantization [49] demonstrate scalability for efficient retrieval from large image databases.

D. Training and Data

Supervised and unsupervised deep learning approaches are both employed in SBIR [49], [57]–[59], with most SBRSIR research using supervised training. In supervised training process, adequately annotated sketch-remote sensing datasets are crucial, with only two dedicated SBRSIR benchmark datasets identified—RSketch [8] and Earth on Canvas [18]. They are relatively small compared to standard SBIR datasets like Quickdraw extend [24] and sketchy [52]. Also, these two datasets only cover a small fraction of all potential sensors. The scarcity of large training data emphasizes the significance of zero-shot and generalization capabilities in SBRSIR—a key improvement in our proposed method.

III. METHODOLOGY

Table I displays the symbols used in this chapter along with their corresponding interpretations.

TABLE I
SYMBOL MARKING CORRESPONDENCE

Symbol	Interpretations
S	Query Sketch
R	Remote sensing image
D^R	Remote sensing image database
E	Visual token embedding
$[RT]$	Retrieval token
Q	Queries in transformers
K	Keys in transformers
V	Values in transformers

Informed by the fundamental principles delineated in prior studies [60] and [13], the proposed model in this research consists of two components: a self-attention module for feature extraction and a cross-attention module for similarity calculation. The structural design of this model is visually

represented in Figure 2, which describes the model's capacity for facilitating the retrieval process across two distinct modalities: remote sensing imagery and sketches. Detailed explications of each module's specific functions and their role

within the model are systematically presented in the following sections.

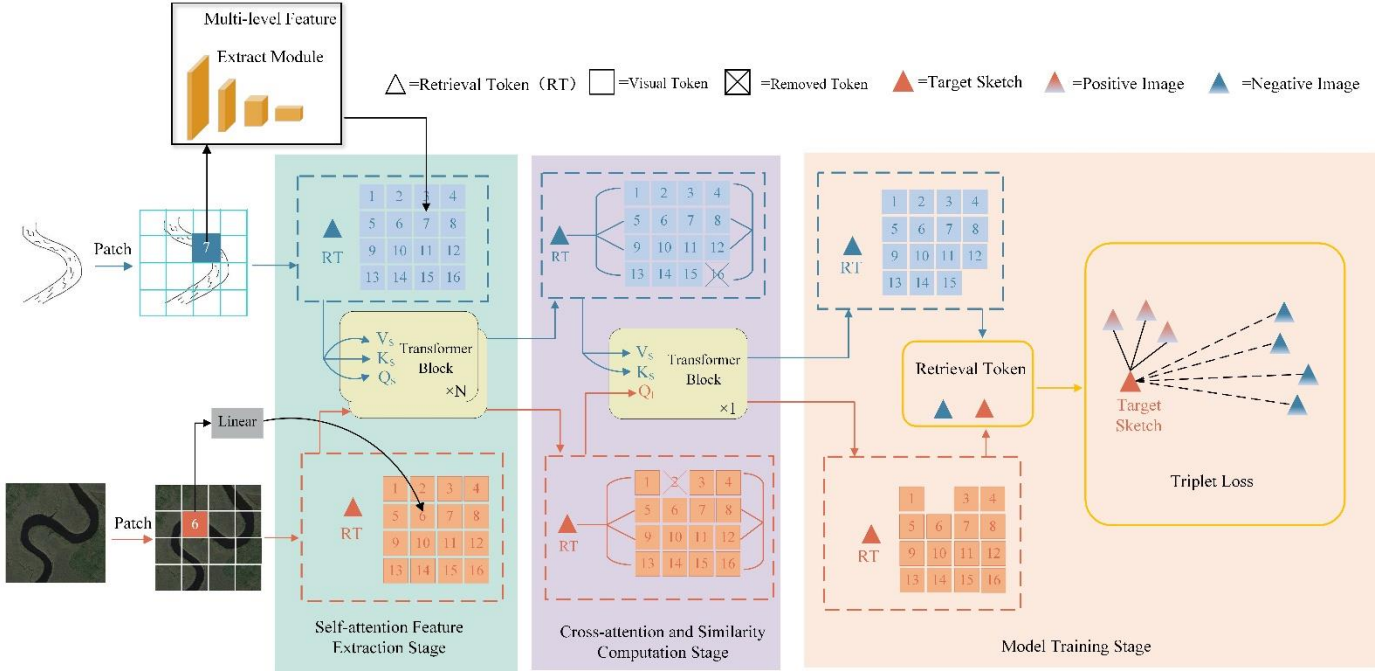


Fig. 2. Network overview: (1) Self-attention feature extraction stage, multi-level extraction and filtering of feature information for different modes. (2) Cross-attention and similarity computation stage, establishing the correspondence of two modes and calculating the similarity (3) Model training stage, train the network using triplet loss.

A. Self-attention Feature Extraction

In the context of sketch-based remote sensing image retrieval, the process typically begins with a query sketch S . The objective is to identify the corresponding remote sensing image R from the remote sensing image database D^R . Traditional deep network methodologies transform hand-drawn sketches and remote sensing images into a sequence of visual tokens. These methods predominantly capture local features of sketches, which are often characterized by sparse strokes, as noted in [13]. To address this limitation and effectively expand the receptive field of visual tokens to better accommodate sparse strokes, this study implements a multi-level feature extraction module applicable to sketches. This enhancement aims to preserve a more comprehensive set of feature information from sketches. The module is constructed by layering multiple convolutional layers with distinct kernel sizes and includes learnable parameters. Following each convolutional layer is a non-linear activation function. This configuration results in an $n \times d$ dimensional visual token embedding $E = [E^1, E^2, \dots, E^n]$, where each E represents a d -dimensional vector.

This module incorporates a transformer-based self-attention mechanism, an approach inspired by the human visual and cognitive systems. This mechanism enables neural networks to dynamically concentrate on the most informative segments within the input data. By integrating the self-attention mechanism, the neural networks in our model are designed to autonomously identify and focus on salient features in the

input, whether it be a sketch or a remote sensing image. This strategy can significantly enhance the network's performance and its ability to generalize.

The initial step in our methodology involves processing the output E from the convolutional layers. This output is first concatenated with a retrieval token $[RT]$, a trainable d -dimensional embedding vector that embodies the global feature. This combination results in an augmented $n+1$ dimensional visual token embedding $E' = [RT, E^1, E^2, \dots, E^n]$. Then, the self-attention is realized by passing E' through first the Multi-Head Self Attention (MSA) module and second the Multi-Layer Perceptron (MLP) module. The forward propagation formula of the model is as follows:

$$E_0 = E' \quad (1)$$

$$E_l = MSA(LN(E_{l-1})) + E_{l-1}, \quad l = 1 \dots L \quad (2)$$

$$E_l = MLP(LN(E_l)) + E_l \quad l = 1 \dots L \quad (3)$$

Formulas (2) and (3) both incorporate residual connections, where L represents the number of hidden attention layers and LN stands for layer normalization.

The MSA module is a core component of our deep network, designed to discern interrelations among various token vectors within a remote sensing image or a sketch. The essential element of this module is the scaled dot-product attention mechanism. Initially, the layer-normalized visual token embedding $E = LN(E_{l-1})$ is multiplied by three learnable

matrices W_q , W_k , and W_v , resulting in Q (Queries), K (Keys), and V (Values) per the following equations:

$$Q = E \cdot W_q, \quad K = E \cdot W_k, \quad V = E \cdot W_v \quad (4)$$

Then the scaled dot-product attention is calculated by the following equation:

$$Attention_{self}(Q, K, V) = softmax(\frac{QK^T}{\sqrt{d}})V \quad (5)$$

In this equation, the product of Q and K assesses the similarity between the Query and Key. The result is then scaled by the square root of the dimension d of E^i to mitigate vanishing gradient problem. A softmax function normalizes the similarities across multiple Keys relative to a Query, ensuring their cumulative sum equals 1. The resulting similarity is used as weights to compute the weighted average of the corresponding V , ultimately obtaining an attention head of $(n+1) \times d$ -dimension. This procedure is replicated h times to create h attention heads. These heads are subsequently integrated into $(n+1) \times d$ -dimensional MSA output by a dense network. The output of MSA is then followed by a MLP module, as described in [60].

The proposed method integrates feature filtering at specific layers of the self-attention module. Given the varying degrees of information richness among local visual tokens generated through self-attention, selectively filtering out tokens with lesser feature information can reduce the number of tokens and improve efficiency for both training and referencing. The filtering is achieved by leveraging attention scores between $[RT]$ and all other visual token embedding vectors. Specifically, the typical Query of visual token embedding is replaced with the Query of $[RT]$. The formula is as follows:

$$Attention_{filtering}(Q, K, V) = softmax(\frac{Q_{[RT]}K^T}{\sqrt{d}}) \quad (6)$$

Utilizing this equation enables the computation of attention scores between $[RT]$ and all visual tokens. Based on the attention scores, only k visual token vectors are retained for further processing. Consequently, this leads to a more refined set of visual token embeddings for both the sketch image and remote sensing images, denoted as $E'' = [RT_{final}, E_{final}^1, \dots, E_{final}^k]$ (where $k < n$).

B. Cross-attention and Similarity Calculation

Unlike conventional methods that map the learned features of both modalities into a unified embedding space, our method employs cross-attention to establish cross-modal token embedding correspondences between sketches and remote sensing images. This involves an interchange of the sketch query Q_S and the candidate remote sensing image query Q_R . After swap, the Query, Key, and Value for the sketch and remote sensing image become (Q_R, K_S, V_S) and (Q_S, K_R, V_R) respectively. This interchange facilitates a direct connection between the visual token embedding sets of the sketches and the remote sensing images. Taking Q_S as an example, the cross-modal attention is obtained using the following formula:

$$Attention_{cross}(Q_S, K_R, V_R) = softmax(\frac{Q_S K_R^T}{\sqrt{d}})V_R \quad (7)$$

Through this attention mechanism, the visual token embeddings of both the sketch and the remote sensing image,

including the retrieval token $[RT]$, are updated based on the pair-wise token information from each modality.

The final step in our methodology involves the use of Euclidean distance between $[RT]_S$ and $[RT]_R$ as a metric for measuring the similarity between the sketch input and a candidate remote sensing image.

C. Model Training and Image Retrieval

In this study, the deep network is trained using the triplet loss function with $[RT]$ derived from both sketches and remote sensing images. Specifically, we consider a triplet (S_i, R_i^+, R_i^-) in the training set, where S_i denotes a query sketch, R_i^+ denotes a remote sensing image with the same label as S_i , and R_i^- denotes a remote sensing image with a different label. The primary aim of this loss function is to minimize the distance between correctly matched sketch-remote sensing image pairs (positive examples) while ensuring that the distance between each sketch and incorrectly matched remote sensing images (negative examples) exceeds a predefined margin. Here, $[RT]$ is used as the global descriptor for sketches and remote sensing images. The triplet loss is defined as the following equation:

$$L_{tri} = \frac{1}{T} \sum_{i=1}^T \max \left\{ \left\| [RT]_{S_i}, [RT]_{R_i^+} \right\|_2 - \left\| [RT]_{S_i}, [RT]_{R_i^-} \right\|_2 + m, 0 \right\} \quad (8)$$

In this equation, T represents the total number of triplets, and m denotes the margin that discriminates whether a sketch and a remote sensing image are from the same class. If a sketch and a candidate remote sensing image's difference exceeds the margin value, they are not in the same class.

In the retrieval phase, the query sketch is processed through the network to obtain its retrieval token $[RT]_S$. Similarly, each candidate remote sensing images in the database are transformed into $[RT]_R$. The similarity between $[RT]$ of the sketch input and a candidate remote sensing image is measured by calculating their Euclidean distance. A smaller Euclidean distance indicates a closer similarity. Subsequently, the remote sensing images that exhibit the smallest distances from the query sketch—essentially, its k -nearest neighbors—are selected as the final output of the model's retrieval process.

To further improve the response speed during actual retrieval operations, $[RT]_R$ is pre-computed and stored in the database by invoking the model in advance. During retrieval, the model is only required to compute the retrieval token for the input sketch. Following this, the pre-stored $[RT]_R$ from the remote sensing image database are rapidly accessed, and the Euclidean distance between $[RT]_S$ and all $[RT]_R$ in the database can be directly calculated. This approach significantly accelerates the retrieval process, especially when dealing with big remote sensing image collections. Moreover, the efficiency of the retrieval process can be further augmented by employing techniques such as approximate nearest neighbor algorithms or utilizing a vector database. This improvement is particularly useful as the volume of images in the remote sensing database expands, underscoring

the practical scalability and efficiency of the model in real-world retrieval scenarios. These mechanisms are crucial for optimizing the model's performance, particularly in retrieval applications where speed and accuracy are paramount.

IV. EXPERIMENTS

A. Dataset

The development of effective cross-modal retrieval models, particularly for sketch-based remote sensing image retrieval (SBR SIR), is hindered by the scarcity of specialized datasets. While there are numerous cross-modal retrieval datasets for natural images, such as Sketchy, TUBerkin, and QuickDraw, the availability of similar datasets for remote sensing images is limited. This gap presents a significant challenge for training SBR SIR models.

This study used RSketch dataset [8], RSketch_Ext dataset (expanded based on RSketch dataset), Earth on canvas dataset [18], and GF-1 image tiles of the Anhui Province section in the middle and lower basin of the Yangtze River. The RSketch dataset, a publicly available sketch-remote sensing image dataset, comprises 20 categories including airplanes, baseball fields, and bridges, each with 45 sketches and 200 remote sensing images. In this study, we expanded the RSketch dataset by augmenting each category with additional remote sensing images sourced from various public datasets like AID [61], NWPU-RESISC45 [62], UCMerge [63], WHU_RS19 [64] and others. Additionally, we enriched the dataset with more sketches obtained from diverse online sources. Post-expansion, each category includes 90 sketches and at least 400 remote sensing images, significantly increasing the dataset's size. Figure 3 presents sample data from each category in the RSketch_Ext dataset. The Earth on Canvas dataset contains 14 categories, five of which are unique compared to those in the

RSketch and RSketch_Ext dataset, with each category comprising 100 sketches and 100 remote sensing images. Table II presents the classes in RSketch, RSketch_Ext and Earth on Canvas dataset. Figure 3 illustrates the sample data corresponding to each category in this dataset. GF-1 images tiles specifically depicted a section of the Yangtze River in Anhui Province, China. There were 4842 image tiles, and each image tile was formatted to a resolution of 256×256 pixels.

TABLE II
CLASSES IN RSKETCH, RSKETCH_EXT, AND EARTH ON CANVAS

RSketch and RSketch_Ext	Earth on Canvas
Airplane	Airplane
Baseball Field	Baseball Field
Golf Course	Golf Course
Intersection	Intersection
Overpass	Overpass
River	River
Runway	Runway
Storage Tanks	Storage Tanks
Tennis Court	Tennis Court
Basketball Field	Buildings
Beach	Freeway
Bridge	Harbor
Closed Road	Mobile Home Park
Crosswalk	Parking Lot
Football Field	
Oil Gas Field	
Railway	
Runway Marking	
Swimming Pool	
Wastewater Treatment Plant (WWTP)	



Fig. 3. Samples in the RSketch_Ext dataset (two sketches and two remote sensing images for each category).

In this study, we implemented a 4-fold cross-validation approach to evaluate our model. The 20 categories from both

the RSketch and RSketch_Ext datasets were divided into four distinct sets of seen and unseen classes. These sets were designated as S1-S4. In each fold, 15 categories are assigned as seen classes and participate in training process, while the remaining 5 categories were reserved as unseen classes, used exclusively for testing. This division ensures that the model can be assessed on its ability to generalize to new, previously unseen classes.

TABLE III
DETAILED FOLDS OF UNSEEN CLASSES

S1	S2	S3	S4
1 airplane	2 baseball diamond	3 basketball court	4 beach
5 bridge	6 closed road	7 crosswalk	8 football field
9 golf course	10 intersection	11 oil gas field	12 overpass
13 railway	14 river	15 runway	16 runway marking
17 storage tank	18 swimming pool	19 tennis court	20 wastewater treatment plant (wwtp)

B. Implementation Details

In this research, the proposed method was implemented using PyTorch framework on a single NVIDIA GeForce RTX 3080Ti GPU. Regarding the preprocessing of sketches and remote sensing images for model training, several steps of preprocessing were undertaken. All images were uniformly scaled to a resolution of 224×224 pixels, conforming to the requirements of the pre-trained model used in this study. Additionally, for sketches, the study removed the white background in the images. This preprocessing step was crucial to eliminate redundant information and allowed the self-attention module to focus more effectively on pertinent feature information.

The kernel size of convolutional layers used in the multi-level feature extraction module was set at 7×7 for the initial convolutional layer, while for the subsequent three layers at 3×3. The stride parameter for all these convolutional layers was uniformly maintained at 2. This configuration resulted in the generation of 196 visual tokens, with each token represented as a 768-dimensional vector.

In terms of architecture, the self-attention module blocks were designed akin to those in the Vision Transformer (ViT), comprising 12 blocks. These blocks were pre-trained networks on the ImageNet-1K dataset [65]. The cross-modal attention module had a single layer with 12 heads.

During training process, the AdamW [66] optimizer was employed, with the learning rate set to 2×10^{-5} to balance efficient training convergence with the need for network stability.

C. Evaluation criteria

The evaluation criteria used in this study are:

1) Mean Average Precision (mAP): This metric is a measure of retrieval accuracy, reflecting the mean area underneath the precision-recall curve in multiple queries.

2) Top-K Accuracy: This metric measures the proportion of correctly retrieved images within the top K results returned by the model. In this research, we specifically evaluate the

The four sets of unseen classes are detailed in Table III. Within each seen class, we adopted a split in each set whereby 50% of the remote sensing images were utilized for training, and the remaining 50% were reserved for testing purposes. This partitioning provides a balanced approach for model training and evaluating, ensuring a comprehensive assessment across a diverse range of categories.

model's performance at three levels: the top 10, top 50, and top 100 retrieved images. These varying levels provide a comprehensive assessment of the model's retrieval accuracy and its ability to rank relevant images effectively.

Both mAP and Top-K Accuracy are critical in evaluating the model's performance in retrieving relevant images from the dataset, offering a multi-dimensional understanding of its effectiveness in various test scenarios.

D. Experiments on RSketch dataset

1) Baseline methods

To verify the effectiveness of the proposed method in this study, we compared the proposed model with the following two baseline methods for cross-modal retrieval:

MR-SBIR [8]: This approach introduces a method for cross-modal retrieval that leverages adversarial learning between sketches and remote sensing image features. It employs a feature generator to map the features of both sketches and remote sensing images into a shared embedding space. A discriminator discerns whether the input features originate from sketches or remote sensing images. The adversarial dynamics between the feature generator and the discriminator facilitate the alignment of feature distributions from different modalities within the embedding space.

DOODLE [67]: This approach introduces a sketch-based image retrieval algorithm that integrates both visual and semantic information to generate image embeddings. These embeddings are subsequently projected onto a shared space. The training of this network involves three distinct loss functions: semantic loss, domain loss, and triplet loss, collectively contributing to the successful execution of cross-modal retrieval tasks.

2) Results

In this study, both the proposed method and its counterparts were initially trained and tested using the RSketch dataset as a benchmark. The final outcomes for each network were obtained by averaging the results across the four folds, as detailed in Table IV.

TABLE IV

TEST RESULT (%) WITH RSKETCH DATASET

	Seen				Unseen			
	mAP	Top-10	Top-50	Top-100	mAP	Top-10	Top-50	Top-100
MR-SBIR	83.75	88.77	85.59	77.20	47.86	57.70	49.96	42.44
DOODLE	49.11	56.67	48.33	23.67	33.24	35.00	33.00	31.50
Ours	98.17	98.5	98.31	95.93	76.62	85.00	79.96	70.01

The data in Table IV reveals that our proposed method attained a mean Average Precision (mAP) of 98.17% and a Top-100 accuracy of 95.93% for seen classes. Notably, the performance gap between our model and the baseline methods was more pronounced in unseen classes, with the proposed method achieving a mAP of 76.62% and a Top-100 accuracy of 70.01%. These results suggest that the method presented in this study significantly surpassed other baseline methods in terms of remote sensing image retrieval accuracy. Also, the remote sensing specific methods performed better than DOODLE, which is designed for ordinary images, highlighting the domain gap between the retrieval of ordinary images and remote sensing images.

3) Ablation study

In our study, we conducted a systematic investigation to determine how various hyperparameters influence the performance of the model. One of the key parameters adjusted was the number of heads in the multi-head attention mechanism. We observed that increasing the head count from 8 to 12 led to a notable improvement of 1.8% in the model's mean Average Precision. Conversely, a reduction in the number of heads from 8 to 4 resulted in a mAP decrease of 2.2%. This finding suggests a direct correlation between the number of heads in the attention mechanism and the retrieval accuracy, with a higher count contributing positively to performance.

Moreover, modifications to the learning rate of the AdamW optimizer also demonstrated significant impacts on the model's retrieval accuracy. An increase in the learning

rate from 1×10^{-5} to 2×10^{-5} yielded a 0.6% increase in the mAP value. In contrast, reducing the learning rate from 1×10^{-5} to 5×10^{-6} led to a substantial decline in mAP, a decrease of 5.9%. These insights highlight the sensitivity of the model to specific hyperparameter settings, underscoring the importance of careful tuning to optimize retrieval performance.

E. Experiments on Rsketch_Ext dataset

In order to assess the influence of both the volume and diversity of training data on the model's capabilities, our study conducted an experiment using the Rsketch_Ext dataset. Compared to Rsketch, this dataset maintains the same number of categories but with a substantially increased quantity of images in each. Notably, these additional images are sourced from a variety of different datasets, providing a broader range of data inputs. The objective of utilizing the Rsketch_Ext dataset was to determine how the inclusion of images from diverse sources impacts the model's ability to accurately retrieve seen and unseen classes during testing.

Maintaining consistency in other settings, we compared the model's performance when trained and tested with both the Rsketch and Rsketch_Ext datasets. The outcomes of these tests are presented in Table V. This comparison aims to shed light on the relationship between training data characteristics – particularly in terms of volume and source diversity – and the model's efficacy.

TABLE V
MODEL RESULTS (%) BEFORE AND AFTER DATASET EXPANSION

	Seen				Unseen			
	mAP	Top10	Top50	Top100	mAP	Top10	Top50	Top100
RSketch	98.17	98.50	98.31	95.93	76.62	85.00	79.96	70.01
RSketch_Ext	98.51	99.33	99.49	99.45	69.59	82.00	80.62	78.20

From Table V, it can be observed that the model trained and tested using the extended dataset showed a slight improvement in retrieval accuracy for seen classes compared to the model trained on the original RSketch dataset. This is mainly because the model trained on the original dataset already achieved high accuracy for seen classes, leaving little room for further improvement. However, in the retrieval of unseen classes, the model trained on the expanded dataset exhibits a decrease of 7% in mAP value and a decrease of approximately 3% in

Top10 accuracy compared to the model trained on the original dataset. The values for Top50 showed minimal changes, while there was an increase of around 8% in Top100 accuracy. The reason for this result may be attributed to the expansion of both the training and testing sets after expanding the dataset. With an increase in the number of images per category, the difficulty of retrieval also increases, leading to a decrease in mAP value for unseen classes.

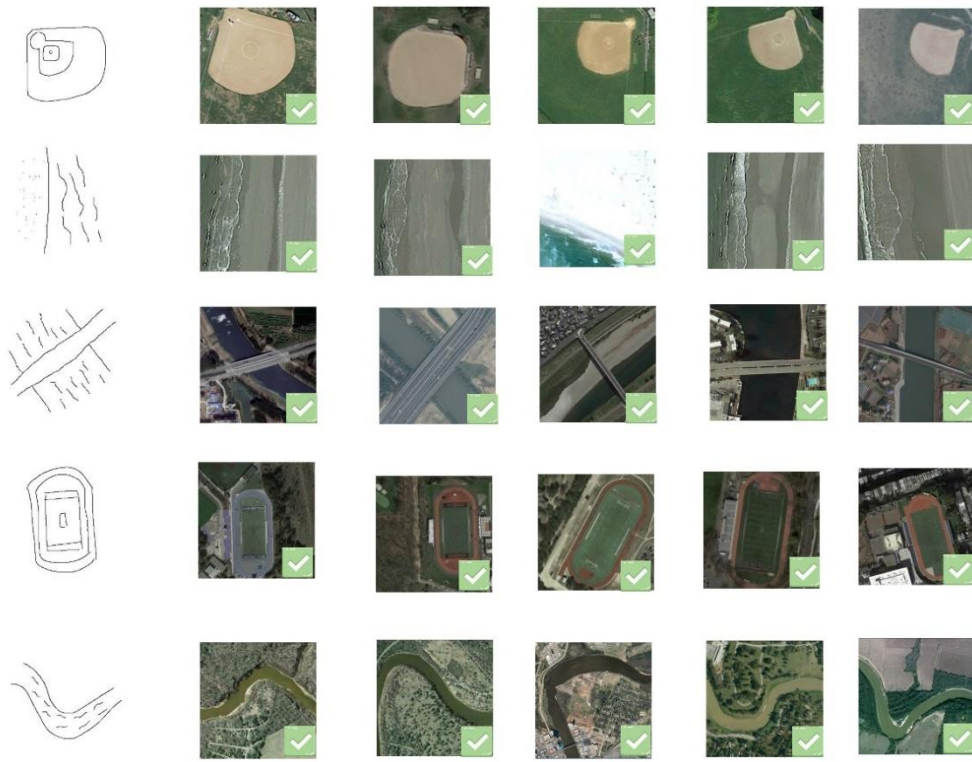


Fig. 4. Retrieval results of 5 seen categories in a test on RSketch_Ext dataset with the top 5 retrieval results. The green checkmark in the lower right corner of the picture marks the correct retrieval, and the red X in the lower right corner marks the wrong retrieval. The five categories selected are baseball diamond, beach, bridge, football field, and river.

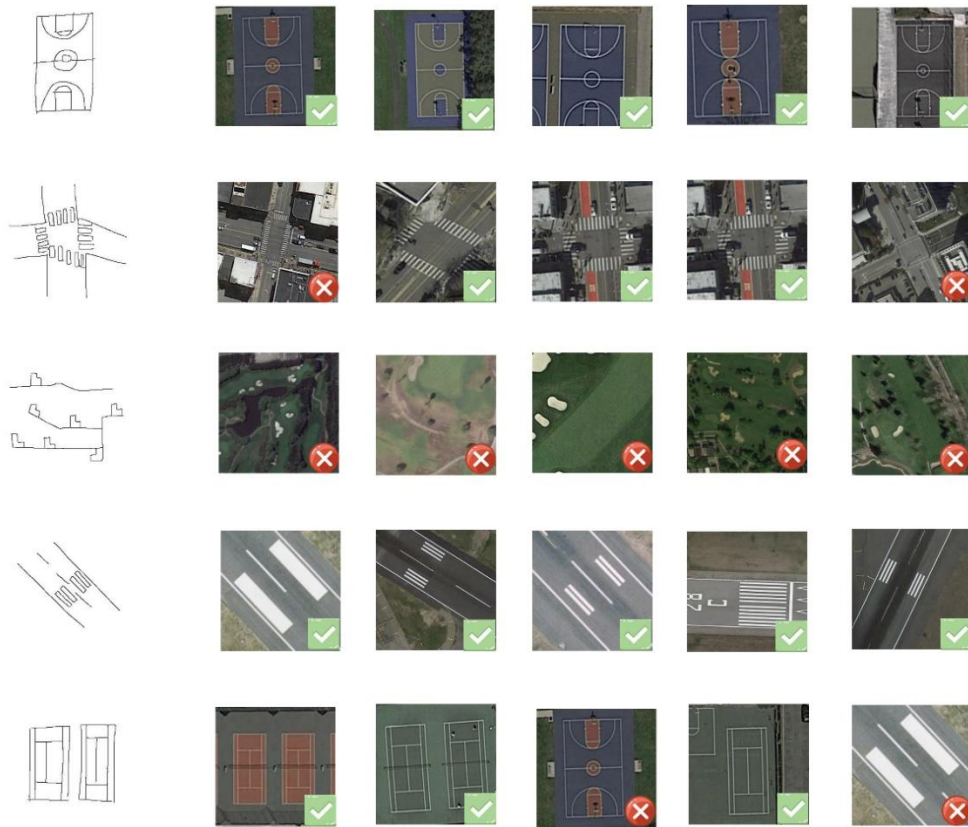


Fig. 5. Retrieval results of 5 unseen categories in a test on RSketch_Ext dataset with the top 5 retrieval results. The green checkmark in the lower right corner of the picture marks the correct retrieval, and the red X in the lower right corner marks the wrong retrieval. The five categories selected are basketball court, crosswalk, oil gas field, runway, and tennis court.

In addition to quantitative analysis, we conducted a manual examination of the retrieval results. Figures 4 and 5 display selected results of our model for both seen and unseen classes within the RSketch_Ext dataset. It is evident that the proposed method achieves high accuracy in retrieving seen classes. Notably, in certain unseen categories such as basketball courts and running tracks, the model also demonstrates high correct retrieval rates. Although there were two instances of incorrect retrievals in the crosswalk category, a closer inspection revealed that the incorrectly retrieved images did indeed feature crosswalk, albeit categorized under ‘intersection’ in the test dataset. While the retrieval results for the oil and gas field category were not accurate, there was a noticeable similarity in texture and structure between the sketches and the retrieved remote sensing images.

TABLE VI
MODEL TEST RESULTS (%) ON EARTH ON CANVAS DATASET

	mAP	Top10	Top50	Top100
S1	63.42	72.86	66.89	56.89
S2	59.65	60.71	57.26	53.69
S3	66.19	73.00	68.43	61.29
S4	70.76	75.71	72.49	65.54
Average	65.01	70.57	66.27	59.35

The results, as presented in Table VI, indicated that the models trained on the RSketch_Ext dataset exhibited good performance when tested on the Earth on Canvas dataset. Notably, the average mean Average Precision (mAP) value achieved is 65.01%, and the Top-10 accuracy reaches 70.57%. These results demonstrated the robust generalization ability of the proposed model, particularly in its capacity to effectively retrieve relevant data from a dataset comprising previously unseen classes and data. This underscored the model's adaptability and potential for practical application in diverse and novel retrieval scenarios.

G. Experiments on GF-1 tiles

In this part of the study, we further evaluated the practical application of the model trained on the RSketch_Ext dataset

F. Experiments on Earth on Canvas dataset

In order to evaluate the generalization capabilities of the proposed model, we conducted an experiment where the model, initially trained on the RSketch_Ext dataset, was subsequently tested on an entirely different dataset, Earth on Canvas. Notably, there are some discrepancies in the class categories between the RSketch_Ext and Earth on Canvas datasets, as presented in Table II. The testing outcomes, including the average accuracy of each fold when applied to the Earth on Canvas dataset, are detailed in Table VI. This approach of testing under zero-shot conditions and across differing datasets provides valuable insights into the model's adaptability and its ability to generalize beyond its training dataset, offering a stringent test of its practical applicability in real-world scenarios.

by conducting retrieval experiments using real-world remote sensing image tiles. As illustrated in Figure 6, the remote sensing image tiles utilized for these experiments were from the GF-1 satellite. For the retrieval input, sketches from the RSketch_Ext dataset were employed. It is important to note that the GF-1 satellite imagery is not part of the training data. Consequently, this set of experiments is a valuable test of the model's capabilities in handling completely unseen data. The use of real satellite imagery in these tests provided a stringent assessment of the model's retrieval accuracy and generalizability in realistic scenarios with remote sensing image tiles of a large research region, beyond the confines of the training dataset.

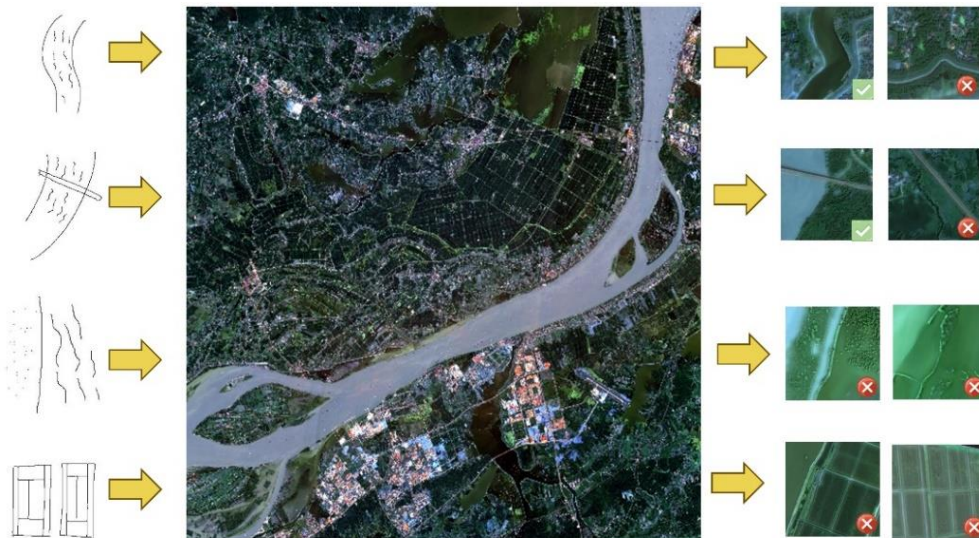


Fig. 6. Retrieval results of GF-1 image tiles

Figure 6 showcases the retrieval capabilities of the proposed model when applied to GF-1 remote sensing image tiles, particularly focusing on river and bridge classes. Despite the model's proficiency in retrieving relevant images, it is noteworthy that some retrieved images, while not precisely matching the query's class, bear a resemblance in shape and texture to the input sketches. This is particularly evident in the retrieval attempts for the beach and tennis court classes, which are not presented in the selected research area. Although the images returned for these categories do not strictly belong to the specified classes, they share a similarity in shape with the sketches used for retrieval. Our method also demonstrates very good retrieval efficiency as it finishes retrieval for 100 sketches inputs in 11.7 seconds.

This observation underlines a significant aspect of the proposed model's functionality: its ability to discern and match shapes between sketches and remote sensing images, exceeding mere categorical correspondence. This capability is particularly useful in instances where the category depicted in the queried sketch is absent from the dataset. In such cases, the model suggests alternative images that, while not categorically identical, are visually similar to the sketch in terms of shape. This outcome indicates the model's potential for broader applications, where shape recognition plays a crucial role in retrieval processes.

V. DISCUSSION

The method introduced in this study, incorporating multi-level feature extraction and attention-guided tokenization, offers a novel deep learning approach to for Sketch-Based Remote Sensing Image Retrieval. Our findings demonstrated the effectiveness of this method, which outperformed two baseline methods, particularly under zero-shot conditions. Additionally, the method exhibited good generalization capabilities. It could effectively handle remote sensing images from sources not included in the training dataset, thus underscoring its robustness and flexibility. A notable feature of the proposed method is the pre-computation of retrieval tokens for each remote sensing image in the database, enabling accelerated retrieval processes through vector search algorithms.

Despite ablation studies and the promising results from experiments across four datasets, further exploration of the network's full potential remains pertinent. For instance, the current approach utilizes multi-level tokenization for sketches and applies identical token filtering mechanisms for both sketches and remote sensing images, which could be optimized separately for each modality. Moreover, leveraging the latest pre-trained networks could enhance the self-attention model. Our current training process begins with a network pre-trained on the ImageNet-1K dataset. Exploring other cutting-edge pre-trained networks may yield additional improvements.

For experiment dataset, the study's expansion of the RSketch dataset to RSketch_Ext focuses primarily on increasing the volume and diversity of sketches and remote sensing images per class, rather than expanding the range of

scenario classes. Given that the current 20 classes are insufficient to encompass all potential scenarios, a significant expansion of the training dataset's class diversity is necessary but poses challenges in terms of time and resources. An automated approach for extending the benchmark dataset would be invaluable for future research in this domain.

The sketches used in this study were limited to uniform line strokes, yet sketches can vary widely in form, including variations in line width, texture depiction, and annotations. Investigating how to adapt our model to accommodate these diverse sketch forms presents an intriguing avenue for future research. Incorporating sketch annotations could introduce a natural language modality, transitioning from current two-modality to a three-modality SBRSIR framework. Furthermore, our tests with GF-1 image tiles suggest potential of our model for fine-grained retrieval, making further investigation and enhancement of the model for fine-grained remote sensing image retrieval plausible.

VI. CONCLUSION

In this paper, we introduce a novel zero-shot sketch-based remote sensing image retrieval method, leveraging multi-level feature extraction and attention-guided tokenization. The efficacy of this method has been thoroughly evaluated through experiments conducted on four remote sensing datasets. The results clearly indicate that our method not only surpasses other baseline methods but also exhibits strong zero-shot learning and generalization capabilities. Particularly noteworthy is the network's ability to retrieve remote sensing images from both unseen categories and unseen data sources. Our model is especially relevant for large-scale remote sensing datasets, as it enables the pre-calculation of retrieval tokens for all images in a database, enhancing scalability. Another significant contribution of this research is the manual expansion of the RSketch dataset into the RSketch_ext dataset. This expansion, which substantially increases both the volume and diversity of the dataset, provides valuable insights into the performance of SBRSIR algorithms. We have made both the code of our method and the RSketch_ext dataset publicly available online. This initiative aims to enable and encourage ongoing research and innovation in the area of sketch-based remote sensing image retrieval.

ACKNOWLEDGMENT

We would like to thank Anhui Province Key Laboratory of Wetland Ecosystem Protection and Restoration, Anhui University to provide us the hardware necessary for this project. We also thank the Space Climate Observatory Habitat Yangtze project, as this model is one of the project's outcomes.

REFERENCES

- [1] Y. Li, J. Ma, Y. Zhang, "Image retrieval from remote sensing big data: A survey," *Information Fusion*, vol. 67, pp. 94-115, 2021.

- [2] X. Yuan, J. Shi, L. Gu, "A review of deep learning methods for semantic segmentation of remote sensing imagery," *Expert Systems with Applications*, vol. 169, pp. 114417, 2021.
- [3] X. Zhang, Y. Zhou, J. Luo, "Deep learning for processing and analysis of remote sensing big data: A technical review," *Big Earth Data*, vol. 6, no. 4, pp. 527-560, 2022.
- [4] W. Zhou, S. Newsam, C. Li et al., "PatternNet: A benchmark dataset for performance evaluation of remote sensing image retrieval," *ISPRS journal of photogrammetry and remote sensing*, vol. 145, pp. 197-209, 2018.
- [5] X. Li, J. Yang, J. Ma, "Recent developments of content-based image retrieval (CBIR)," *Neurocomputing*, vol. 452, pp. 675-689, 2021.
- [6] C. Liu, J. Ma, X. Tang et al., "Deep hash learning for remote sensing image retrieval," *IEEE Transactions on Geoscience and Remote Sensing*, vol. 59, no. 4, pp. 3420-3443, 2020.
- [7] T. Abdullah, Y. Bazi, A. Rahhal et al., "TextRS: Deep bidirectional triplet network for matching text to remote sensing images," *Remote Sensing*, vol. 12, no. 3, pp. 405, 2020.
- [8] F. Xu, W. Yang, T. Jiang et al., "Mental Retrieval of Remote Sensing Images via Adversarial Sketch-Image Feature Learning," *IEEE Transactions on Geoscience and Remote Sensing*, vol. 99, pp. 1-14, 2020.
- [9] Q. Yu, F. Liu, Y. Song et al., "Sketch me that shoe," in *IEEE-CVPR*, Las Vegas, Nevada, USA, 2016, pp. 799-807.
- [10] P. Xu, T. M. Hospedales, Q. Yin et al., "Deep learning for free-hand sketch: A survey," *IEEE transactions on pattern analysis and machine intelligence*, vol. 45, no. 1, pp. 285-312, 2022.
- [11] A. Chaudhuri, A. K. Bhunia, Y. Song et al., "Data-Free Sketch-Based Image Retrieval," in *Proc. IEEE-CVPR*, Vancouver, British Columbia, Canada, 2023, pp. 12084-12093.
- [12] P. N. Chowdhury, A. K. Bhunia, A. Sain et al., "SceneTrilogy: On Human Scene-Sketch and its Complementarity with Photo and Text," in *Proc. IEEE-CVPR*, Vancouver, British Columbia, Canada, 2023, pp. 10972-10983.
- [13] F. Lin, M. Li, D. Li et al., "Zero-Shot Everything Sketch-Based Image Retrieval, and in Explainable Style," in *Proc. IEEE-CVPR*, Vancouver, British Columbia, Canada, 2023, pp. 23349-23358.
- [14] A. Sain, A. K. Bhunia, P. N. Chowdhury et al., "Clip for all things zero-shot sketch-based image retrieval, fine-grained or not," in *Proc. IEEE-CVPR*, Vancouver, British Columbia, Canada, 2023, pp. 2765-2775.
- [15] A. Sain, A. K. Bhunia, Y. Yang et al., "Stylemeup: Towards style-agnostic sketch-based image retrieval," in *IEEE-CVPR*, Kuala Lumpur, Selangor, Malaysia, 2021, pp. 8504-8513.
- [16] W. Chen, Y. Liu, W. Wang et al., "Deep learning for instance retrieval: A survey," *IEEE Transactions on Pattern Analysis and Machine Intelligence*, 2022.
- [17] D. Yu, Y. Liu, Y. Pang et al., "A multi-layer deep fusion convolutional neural network for sketch based image retrieval," *Neurocomputing*, vol. 296, pp. 23-32, 2018.
- [18] U. Chaudhuri, B. Banerjee, A. Bhattacharya et al., "A zero-shot sketch-based intermodal object retrieval scheme for remote sensing images," *IEEE Geoscience and Remote Sensing Letters*, vol. 19, pp. 1-5, 2021.
- [19] U. Chaudhuri, R. Bose, B. Banerjee et al., "Zero-shot cross-modal retrieval for remote sensing images with minimal supervision," *IEEE Transactions on Geoscience and Remote Sensing*, vol. 60, pp. 1-15, 2022.
- [20] U. Chaudhuri, B. Banerjee, A. Bhattacharya et al., "A simplified framework for zero-shot cross-modal sketch data retrieval," in *IEEE-CVPR*, Seattle, Washington, USA, 2020, pp. 182-183.
- [21] T. Jiang, G. Xia, Q. Lu, "Sketch-based aerial image retrieval," *IEEE-ICIP*, Beijing, China, 2017, pp. 3690-3694.
- [22] F. Xu, R. Zhang, W. Yang et al., "Mental retrieval of large-scale satellite images via learned sketch-image deep features," in *IEEE-IGARSS*, Yokohama, Japan, 2019, pp. 3356-3359.
- [23] R. Hu, J. Collomosse, "A performance evaluation of gradient field hog descriptor for sketch based image retrieval," *Computer Vision and Image Understanding*, vol. 117, no. 7, pp. 790-806, 2013.
- [24] D. Ha, D. A. Eck, "Neural Representation of Sketch Drawings," 2017, arXiv: 1704.03477.
- [25] F. Huang, J. F. Canny, J. Nichols, "Swire: Sketch-based user interface retrieval," in *ACM-CHI*, Glasgow, UK, 2019, pp. 1-10.
- [26] M. Bertolotto, J. D. Carswell, E. McLoughlin et al., "Using sketches and knowledge bases for geo-spatial image retrieval," *Computers, environment and urban systems*, vol. 30, no. 1, pp. 29-53, 2006.
- [27] S. K. Yelamarthi, S. K. Reddy, A. Mishra et al., "A zero-shot framework for sketch based image retrieval," in *Springer-ECCV*, Munich, Germany, 2018, pp. 300-317.
- [28] A. K. Bhunia, Y. Yang, T. M. Hospedales et al., "Sketch less for more: On-the-fly fine-grained sketch-based image retrieval," in *IEEE-CVPR*, Seattle, Washington, USA, 2020, pp. 9779-9788.
- [29] C. H. Lampert, H. Nickisch, S. Harmeling, "Attribute-based classification for zero-shot visual object categorization," *IEEE transactions on pattern analysis and machine intelligence*, vol. 36, no. 3, pp. 453-465, 2013.
- [30] Z. Zhang, V. Saligrama, "Zero-shot learning via semantic similarity embedding," in *IEEE-ICCV*, Santiago, Chile, 2015, pp. 4166-4174.
- [31] K. Pang, K. Li, Y. Yang et al., "Generalising fine-grained sketch-based image retrieval," in *IEEE-CVPR*, Long Beach, California, USA, 2019, pp. 677-686.
- [32] S. D. Bhattacharjee, J. Yuan, Y. Huang et al., "Query adaptive multiview object instance search and localization using sketches," *IEEE Transactions on Multimedia*, vol. 20, no. 10, pp. 2761-2773, 2018.
- [33] J. M. Saavedra, "Sketch based image retrieval using a soft computation of the histogram of edge local orientations (s-helo)," in *IEEE-ICIP*, Paris, France, 2014, pp. 2998-3002.
- [34] T. Dutta, S. Biswas, "s-sbir: Style augmented sketch based image retrieval," in *IEEE-WACV*, Aspen, Colorado, USA, 2020, pp. 3261-3270.
- [35] L. Zheng, Y. Yang, Q. Tian, "SIFT meets CNN: A decade survey of instance retrieval," *IEEE transactions on pattern analysis and machine intelligence*, vol. 40, no. 5, pp. 1224-1244, 2017.
- [36] J. Jiang, R. Wang, S. Lin et al., "Sfsegnet: Parse freehand sketches using deep fully convolutional networks," in *IEEE- IJCNN*, Budapest, Hungary, 2019, pp. 1-8.
- [37] F. Wang, Y. Li, "Spatial matching of sketches without point correspondence," in *IEEE-ICIP*, Quebec, Canada, 2015, pp. 4828-4832.
- [38] K. Li, K. Pang, Y. Song et al., "Toward deep universal sketch perceptual grouper," *IEEE Transactions on Image Processing*, vol. 28, no. 7, pp. 3219-3231, 2019.
- [39] P. Xu, C. K. Joshi, X. Bresson, "Multigraph transformer for free-hand sketch recognition," *IEEE Transactions on Neural Networks and Learning Systems*, vol. 33, no. 10, pp. 5150-5161, 2021.
- [40] H. Lin, Y. Fu, X. Xue et al., "Sketch-bert: Learning sketch bidirectional encoder representation from transformers by self-supervised learning of sketch gestalt," in *IEEE-CVPR*, Seattle, Washington, USA, 2020, pp. 6758-6767.
- [41] J. Lei, Y. Song, B. Peng et al., "Semi-heterogeneous three-way joint embedding network for sketch-based image retrieval," *IEEE Transactions on Circuits and Systems for Video Technology*, vol. 30, no. 9, pp. 3226-3237, 2019.
- [42] H. Zhang, C. Zhang, M. Wu, "Sketch-based cross-domain image retrieval via heterogeneous network," in *IEEE-VCIP*, Petersburg, Florida, USA, 2017, pp. 1-4.
- [43] B. Chen, W. Deng, "Hybrid-attention based decoupled metric learning for zero-shot image retrieval," in *IEEE-CVPR*, Long Beach, California, USA, 2019, pp. 2750-2759.
- [44] W. Kim, B. Goyal, K. Chawla et al., "Attention-based ensemble for deep metric learning," in *Springer-ECCV*, Munich, Germany, 2018, pp. 736-751.
- [45] Y. Liang, C. Ge, Z. Tong et al., "Not All Patches are What You Need: Expediting Vision Transformers via Token Reorganizations," 2022, arXiv: 2202.07800.
- [46] F. Liu, C. Zou, X. Deng et al., "Scenesketcher: Fine-grained image retrieval with scene sketches," in *Springer-ECCV*, Copenhagen, Denmark, 2020, pp. 718-734.
- [47] H. Jégou, F. Perronnin, M. Douze et al., "Aggregating local image descriptors into compact codes," *IEEE transactions on pattern analysis and machine intelligence*, vol. 34, no. 9, pp. 1704-1716, 2012.
- [48] E. Spyromitros-Xioufis, S. Papadopoulos, I. Y. Kompatsiaris et al., "A Comprehensive Study Over VLAD and Product Quantization in Large-Scale Image Retrieval," *IEEE Transactions on Multimedia*, vol. 16, no. 6, pp. 1713-1728, 2014.
- [49] P. Xu, Y. Huang, T. Yuan et al., "Sketchmate: Deep hashing for million-scale human sketch retrieval," in *IEEE-CVPR*, Salt Lake City, Utah, USA, 2018, pp. 8090-8098.
- [50] Y. Shen, L. Liu, F. Shen et al., "Zero-shot sketch-image hashing," in *IEEE-CVPR*, Salt Lake City, Utah, USA, 2018, pp. 3598-3607.
- [51] T. Jiang, G. Xia, Q. Lu et al., "Retrieving aerial scene images with learned deep image-sketch features," *Journal of Computer Science and Technology*, vol. 32, pp. 726-737, 2017.
- [52] L. Liu, F. Shen, Y. Shen et al., "Deep sketch hashing: Fast free-hand sketch-based image retrieval," in *IEEE-CVPR*, Honolulu, Hawaii, USA, 2017, pp. 2862-2871.

- [53] H. Zhao, M. Liu, M. Li, "Feature Fusion and Metric Learning Network for Zero-Shot Sketch-Based Image Retrieval," *Entropy*, vol. 25, no. 3, pp. 502, 2023.
- [54] G. Dai, J. Xie, Y. Fang, "Deep correlated holistic metric learning for sketch-based 3D shape retrieval," *IEEE Transactions on Image Processing*, vol. 27, no. 7, pp. 3374-3386, 2018.
- [55] W. Zhou, H. Li, Y. Lu et al., "Large scale image search with geometric coding," in *the 19th ACM international conference on Multimedia*, Scottsdale, Arizona, USA, 2011, pp. 1349-1352.
- [56] Y. Matsui, K. Ito, Y. Aramaki et al., "Sketch-based manga retrieval using manga109 dataset," *Multimedia Tools and Applications*, vol. 76, pp. 21811-21838, 2017.
- [57] J. He, X. Wu, Y. Jiang et al., "Sketch recognition with deep visual-sequential fusion model," in *the 25th ACM international conference on Multimedia*, Silicon Valley, California, USA, 2017, pp. 448-456.
- [58] P. Xu, Z. Song, Q. Yin et al., "Deep self-supervised representation learning for free-hand sketch," *IEEE Transactions on Circuits and Systems for Video Technology*, vol. 31, no. 4, pp. 1503-1513, 2020.
- [59] A. Creswell, A. A. Bharath, "Adversarial training for sketch retrieval," in *Springer-ECCV*, Amsterdam, Holland, 2016, pp. 798-809.
- [60] A. Dosovitskiy, L. Beyer, A. Kolesnikov et al., "An Image is Worth 16x16 Words: Transformers for Image Recognition at Scale," in *IMLS-ICLR*, [Online], 2021, arXiv: 2010.11929.
- [61] G. Xia, J. Hu, F. Hu et al., "AID: A benchmark data set for performance evaluation of aerial scene classification," *IEEE Transactions on Geoscience and Remote Sensing*, vol. 55, no. 7, pp. 3965-3981, 2017.
- [62] G. Cheng, J. Han, X. Lu, "Remote sensing image scene classification: Benchmark and state of the art," *Proceedings of the IEEE*, vol. 105, no. 10, pp. 1865-1883, 2017.
- [63] Y. Yang, S. Newsam, "Geographic image retrieval using local invariant features," *IEEE transactions on geoscience and remote sensing*, vol. 51, no. 2, pp. 818-832, 2012.
- [64] G. Sheng, W. Yang, T. Xu et al., "High-resolution satellite scene classification using a sparse coding based multiple feature combination," *International journal of remote sensing*, vol. 33, no. 8, pp. 2395-2412, 2012.
- [65] J. Deng, W. Dong, R. Socher et al., "Imagenet: A large-scale hierarchical image database," in *IEEE-CVPR*, Miami, Florida, USA, 2009, pp. 248-255.
- [66] I. Loshchilov, F. Hutter, "Fixing weight decay regularization in adam," 2017, arXiv: 1711.05101.
- [67] S. Dey, P. Riba, A. Dutta et al., "Doodle to search: Practical zero-shot sketch-based image retrieval," in *IEEE-CVPR*, Long Beach, California, USA, 2019, pp. 2179-2188.



Xiaoshuang Ma (Member, IEEE) received the Ph.D. degree in cartography and geographic information engineering from Wuhan University, Wuhan, China, in 2016.

He is an Associate Professor with the Department of Resources and Environmental Engineering, Anhui University, Hefei, China. His research interest includes synthetic aperture radar (SAR) image processing and interpretation.



Beiping Song, receive the B.S. degree in environmental engineering from Chizhou University, Chizhou, China, in 2022. He is pursuing the M.S. degree in resources and environment with Anhui University, Hefei, China.

His research interests cover deep learning, remote sensing and image retrieval.



Zhuang Liu, receive the B.S. degree in geographic information system from Xinjiang University, Urumqi, China, in 2007. He is currently employed as the Manager of the Software Development Department in the Delivery Center at Shanghai Ubiquitous Navigation Technology Co. Ltd.



Bo Yang receive the B.S. degree in environmental engineering from Henan University of Engineering, Zhengzhou, China, in 2020. He is pursuing the M.S. degree in resources and environment with Anhui University, Hefei, China.

His research interests include deep learning, remote sensing and pattern recognition.



Chen Wang (Member, IEEE), received his Ph.D diploma at the Department of Geomatics Sciences at Universite Laval, Quebec, Canada. He is currently lecturer at the Department of Geo-information and Geomatics, Anhui University, China. His current research topic is GeoAI and Remote sensing data processing.